Earth's Future

RESEARCH ARTICLE
10.1029/2023EF003590

Coupling GEDI LiDAR and Optical Satellite for Revealing Large-Scale Maize Lodging in Northeast China

Qiang Zhang[1,2,3], Geli Zhang[1], Yao Zhang[4], Xiangming Xiao[5], Nanshan You[2], Zhichao Li[2], Hao Tang[6], Tong Yang[1], Yuanyuan Di[1,2], and Jinwei Dong[2,3]

[1]College of Land Science and Technology, China Agricultural University, Beijing, China, [2]Key Laboratory of Land Surface Pattern and Simulation, Institute of Geographic Sciences and Natural Resources Research, Chinese Academy of Sciences, Beijing, China, [3]University of Chinese Academy of Sciences, Beijing, China, [4]Sino-French Institute for Earth System Science, College of Urban and Environmental Sciences, Peking University, Beijing, China, [5]Department of Microbiology and Plant Biology, Center for Earth Observation and Modeling, University of Oklahoma, Norman, OK, USA, [6]Department of Geography, National University of Singapore, Singapore, Singapore

Abstract Wind-induced crop lodging can reduce agricultural production and impact food security. However, a systematic evaluation of large-scale crop lodging and its drivers is lacking, mostly due to the limited observations available. Such knowledge gaps hinder the application of effective management practices to mitigate yield losses. Here, we quantify maize-lodging induced by three consecutive typhoons in Northeast China in 2020 using direct crop canopy height observations from the Global Ecosystem Dynamics Investigations (GEDI) instrument and optical satellite imagery. We show that the canopy water-related vegetation index provides a robust wall-to-wall mapping of crop lodging, supported by changes in GEDI canopy height. Our spatially contiguous lodging maps show that lodging intensity is mainly due to typhoon intensity (64.34%), with maize plantation fraction (11.94%) and phenology (7.94%) as secondary factors. The shelterbelt forest may partly alleviate the lodging risk, but its effect requires further investigation. Considering the recent expansion of maize cultivation and the poleward shift of landfalling typhoons alongside climate change, the lodging risk may increase for maize and further threaten China's food security.

Plain Language Summary Wind-induced crop lodging can substantially reduce agricultural production and jeopardize regional and global food security. However, large-scale characterizations of typhoon-induced crop lodging are limited, hindering the understanding of its overall impacts and driving mechanisms. We show for the first time that the novel space-borne LiDAR and optical satellite data can provide a consistent picture of crop damage caused by typhoons at the regional scale, mainly due to typhoon intensity and maize planting fraction. Future overlap between increased typhoons and maize expansion may further threaten China's food security. Our insights also apply to other major maize-producing regions affected by landfalling typhoons or hurricanes, such as the Midwestern US, and help improve crop lodging monitoring systems and mitigation practices.

Key Points:

- Global Ecosystem Dynamics Investigation footprints can well reveal changes in maize height caused by typhoons in Northeast China
- The land surface water index provides a robust wall-to-wall mapping of crop lodging
- Maize lodging intensity is mainly due to typhoon intensity (64.34%), followed by maize plantation fraction (11.94%) and phenology (7.94%)

Supporting Information:

Supporting Information may be found in the online version of this article.

Correspondence to:

G. Zhang, Y. Zhang and J. Dong,
geli.zhang@cau.edu.cn;
zhangyao@pku.edu.cn;
dongjw@igsnrr.ac.cn

Citation:

Zhang, Q., Zhang, G., Zhang, Y., Xiao, X., You, N., Li, Z., et al. (2024). Coupling GEDI LiDAR and optical satellite for revealing large-scale maize lodging in Northeast China. *Earth's Future*, *12*, e2023EF003590. https://doi.org/10.1029/2023EF003590

Received 18 FEB 2023
Accepted 29 NOV 2023

Author Contributions:

Conceptualization: Qiang Zhang, Geli Zhang, Yao Zhang, Jinwei Dong
Data curation: Qiang Zhang
Formal analysis: Qiang Zhang, Geli Zhang, Yao Zhang, Nanshan You
Funding acquisition: Geli Zhang, Jinwei Dong
Investigation: Qiang Zhang, Geli Zhang, Yao Zhang, Xiangming Xiao, Nanshan You, Zhichao Li, Hao Tang, Tong Yang, Yuanyuan Di, Jinwei Dong
Methodology: Qiang Zhang

1. Introduction

The global population is projected to reach 9.7 billion in 2050 (Godfray et al., 2010; Roser et al., 2013), with a concomitant increase in food demand (van Dijk et al., 2021). Both cropland expansion and improved management are needed to achieve this goal. However, increased extreme weather events are posing a greater threat to global food security in the context of global warming (Emanuel, 2005; Ghil & Vautard, 1991; Hasegawa et al., 2021; Lesk et al., 2016; Ray et al., 2022; Solomon et al., 2009). Northwestern Pacific tropical cyclones, also known as typhoons, are one of the most devastating extreme weather events in East and Southeast Asia (Elsner et al., 2008; Lesk et al., 2016; K. Li & Li, 2011; Parry & Carter, 1989). The associated strong wind and excessive precipitation can cause mechanical damage to the crop stems or failures of the root-soil anchorage systems, a phenomenon known as lodging (Pinthus, 1974). It has been reported that lodging-induced yield losses can be as high as 75% in cereal crops and oilseed rape in the UK (Berry & Spink, 2012; Berry et al., 2013). Future warming may lead to the intensification of typhoons (Elsner et al., 2008; Kossin, 2018) and a poleward shift in their occurrence (Altman et al., 2018; Kossin et al., 2014; Tamarin-Brodsky & Kaspi, 2017). Thus, typhoon (or tropical cyclone)-induced crop lodging in mid-and high-latitude bread-basket regions, such as Northeast China and the Midwestern US, is

Supervision: Geli Zhang, Yao Zhang, Jinwei Dong
Visualization: Qiang Zhang
Writing – original draft: Qiang Zhang, Yao Zhang, Jinwei Dong
Writing – review & editing: Qiang Zhang, Geli Zhang, Yao Zhang, Xiangming Xiao, Jinwei Dong

expected to intensify and threaten regional and global food security (Mei & Xie, 2016; Mendelsohn et al., 2012; Sharmila & Walsh, 2018; Studholme et al., 2022; Webster et al., 2005).

Although typhoons have caused enormous economic loss every year (Weinkle et al., 2018), their impacts on crop lodging have been less investigated due to a lack of timely and accurate observations at large scales. Compared to typhoon-induced flooding, accurate characterization of wind-induced crop lodging is more challenging, partly because typhoon occurrence is unpredictable and field surveys are time-consuming and laborious (Boose et al., 1994; Boutet & Weishampel, 2003; Kupfer et al., 2008; McNulty, 2002; F. Wang & Xu, 2009). Recent advances in remote sensing complement previous site-level observations with airborne photography and space-borne microwave polarimetric data, but these are mostly at the experimental stage. Most of these analyses only cover a relatively small area compared to the area affected by typhoons (Chauhan et al., 2019). The lack of large-scale observations of typhoon crop disturbance restricts crop management decisions for sustainable agricultural production.

Space-borne LiDAR can measure the canopy height of vegetation at a precision of centimeters and is, therefore, a cost-effective technique for understanding the impact of typhoons on crops at large spatial scales (Chambers et al., 2007; de Beurs et al., 2019; Rogan et al., 2011; M. Wang & Xu, 2018; W. Wang et al., 2010; X. Zhang et al., 2013). The Global Ecosystem Dynamics Investigation (GEDI) LiDAR instrument onboard the International Space Station (ISS) provides new opportunities for observing typhoon disturbance by collecting unique data on vegetation canopy structure since its launch in April 2019 (Dubayah et al., 2020). GEDI uses eight tracks to measure the distance between vegetation and sensors, from which the vertical canopy profile and other structure metrics can be obtained (Dubayah et al., 2020). The low Earth orbit of the ISS also allows near-global coverage between 51.6°N and S latitudes with a moderate revisit cycle. Thus, GEDI data is suitable for assessing the impact of typhoons in near real-time, but a wall-to-wall mapping is not possible due to the large gaps between swaths.

As one of the world's golden maize belts, Northeast China contributes 41.92% of China's maize production and is critical for regional and national food security (Figure S1 in Supporting Information S1). Unprecedentedly, three consecutive strong typhoons hit the maize planting areas from August 27 to 8 September 2020, causing large areas of crop lodging and enormous economic loss (Table S1 in Supporting Information S1). Here, we use a combination of LiDAR and optical satellite data to characterize the impacts of typhoons on maize in Northeast China. We use high-frequency optical satellite imagery to calculate a canopy water index to complement this deficiency in spatial coverage. With the resultant spatially contiguous crop lodging map, we further explore the underlying mechanisms of crop lodging using a random forest (RF) algorithm.

2. Materials and Methods

2.1. Vegetation Height Data From the GEDI LiDAR Data Set

The GEDI instrument is the first spaceborne LiDAR instrument specifically optimized to measure vegetation structure within approximately ±51.6° latitude, which illuminates the Earth's surface with footprints of ∼25 m diameter (Dubayah et al., 2020). The GEDI L2A data was used in our analysis, which provides footprint-level relative height (RH) metrics. RH metrics represent the height at which a percentile of the laser's energy is returned relative to the ground and is saved at 1% intervals (Dubayah et al., 2020). We resampled the maize layer to 50 m spatial resolution to help remove GEDI footprints that were not on the corn layer, considering the GEDI footprint data are geolocated with a mean positional error of 10.3 m (Dubayah et al., 2020). GEDI footprints were included in our analysis only when the proportion of maize in the corresponding maize pixel was greater than 50%. This could largely mitigate the impact of non-maize vegetation on our analysis. We extracted the RH95 (the height at which there is 95% of the LiDAR return energy) as the maize height and also filtered out footprints with RH95 greater than 5 m, which may be affected by trees, houses, or other artifacts. The period before the typhoon is defined as 11–26 August 2020, when maize has already reached normal heights. The period after the typhoon is defined as from 9 to 20 September 2020, taking into account the impact of the typical maize harvest (starting on October 10) or potential early harvesting on the observations. As for the period of harvested height of maize, we chose December 1 to December 15, taking into account the uneven timing of maize harvest by individual farmers. Choosing this period in winter also avoids the disturbance of other vegetation. In total, we ended up with 56,804 and 56,826 GEDI shots before (August 11–26) and after (September 9–20) the 2020 typhoons, respectively, which covered almost the entire cornfield in Northeast China.

2.2. Optical Metrics From MODIS Satellite From 2017 to 2020

The daily 500-m MCD43A4 collection 6 Nadir Bidirectional Reflectance Distribution Function- (BRDF-) Adjusted Reflectance (NBAR) data set from MODIS was used to generate land surface water index (LSWI), which has been proven to be suitable for vegetation dynamics monitoring (Brandt et al., 2016; Hilker et al., 2012; Z. Li et al., 2018; Norris & Walker, 2020; Schaaf et al., 2002). In this study, we obtained all available MCD43A4 collection 6 NBAR data from 2017 to 2020. This product is retrieved daily and showcases the most optimal BRDF achievable based on the 16 days' worth of inputs with the day of interest emphasized. It excels in quality at higher latitudes due to the comprehensive integration of all available observations throughout the acquisition period. We further adopted the method of Maximum Value Composites to synthesize the data to the 8-day temporal resolution to avoid interference from outlier observations. All data processing was conducted on the Google Earth Engine platform. LSWI was calculated by using the following formula:

$$\mathrm{LSWI} = \frac{\rho_{\mathrm{nir}} - \rho_{\mathrm{swir}}}{\rho_{\mathrm{nir}} + \rho_{\mathrm{swir}}} \quad (1)$$

where ρ_{nir} and ρ_{swir} represent the surface reflectance for the near-infrared and shortwave-infrared bands, respectively.

In addition to LSWI, we also used NDVI, EVI, $\mathrm{NIR_V}$, and the CSIF data set as proxies of vegetation greenness and gross primary production (GPP) (Shekhar et al., 2022; Y. Zhang, Joiner, et al., 2018; Y. Zhang, Xiao, et al., 2018). NDVI, EVI, and $\mathrm{NIR_V}$ were calculated based on the MCD43A4 collection 6 data sets. The CSIF data set is generated by a neural network trained with surface reflectance from MODIS and SIF from the Orbiting Carbon Observatory-2 (OCO-2) (Y. Zhang, Joiner, et al., 2018; Y. Zhang, Xiao, et al., 2018). The CSIF data set has very high consistency with OCO-2 SIF (Y. Zhang, Joiner, et al., 2018; Y. Zhang, Xiao, et al., 2018). The clear-sky daily SIF from the CSIF data set with a 0.05° spatial and 4-d temporal resolution was used in our study, which has a strong correlation with satellite observation and eddy covariance-estimated GPP (Y. Zhang, Joiner, et al., 2018; Y. Zhang, Xiao, et al., 2018).

2.3. Annual Maps of Maize Crop

We acquired the spatial distribution of maize fields from the recent 10-m crop type maps in Northeast China during 2017–2019 (You et al., 2021), which has an overall accuracy of 86%. To avoid the impact of the crop rotation system, we overlaid the 3 years of crop maps and selected persistent maize pixels throughout the 3 years to generate the maize map for our study region. This accurate maize map helps us match the GEDI footprints and optical data, thus minimizing signal interference from other vegetation. Considering the coarser resolution of the MODIS data, we aggregated the 10-m maize layer to the area proportion map of maize at the 500 m spatial resolution to match the MODIS data and then removed the pixels with a maize proportion under 50% to alleviate the effect of mixed pixels (Figure S2 in Supporting Information S1). We did the same processing when matching CSIF data. The maize in Northeast China is widespread in plain areas, as shown in Figure S3 of Supporting Information S1. Northeast China has a cold temperate and humid/sub-humid climate, which allows for one crop per year in this region. The growth period of maize is from mid-May to early October in Northeast China (Figure S4 in Supporting Information S1). We used all proportions of maize as input variables for the machine learning model to better explore the effects of maize fraction on lodging.

2.4. Typhoon-Related Climate Data Sets

The Typhoon Network of the Central Meteorological Observatory (http://typhoon.nmc.cn/) provides hourly information on the location, maximum winds, and central pressure. We acquired the point information of the typhoon records, which indicates when and where the center of the typhoons was located. Those points were used to generate the routes of the three typhoons to track the typhoons across Northeast China (Figure S5 in Supporting Information S1). The three typhoons (Bavi, Maysak, and Haishen) entered Northeast China on 27 August, 3 September, and 8 September 2020, and stayed for 9, 27, and 5 hr, respectively. Typhoon Maysak had the longest residence time and strongest impact on the crops (Figure S5 and Table S1 in Supporting Information S1).

Heavy rainfall and strong wind are the two major forces for crop damage caused by typhoons. Here we used them to represent the meteorological anomalies caused by typhoons. The site-based daily precipitation and maximum

wind speed were provided by the China Meteorological Science Data Center (CMSDC) (http://data.cma.cn/). We first rescaled the daily total precipitation and maximum wind speed data to 8-day data to match the MODIS data for all weather stations. We then interpolated the site data to the regional raster maps using the simple kriging interpolation method (Oliver & Webster, 1990) and finally used the maize layer as a mask to extract the total precipitation and maximum wind speed of each maize pixel during the typhoon.

2.5. Characterizing the Impacts of Typhoons on Maize in Terms of Crop Canopy

Previous studies mainly employed the difference between the two images before and after typhoon events to quantify the disturbances (Abbas et al., 2020; Feng et al., 2020; Negrón-Juárez et al., 2014; Tran et al., 2016). This approach has some pitfalls due to the selection of the post-typhoon image for assessing the vegetation disturbance, and how to disentangle the typhoon-induced vegetation change from seasonal vegetation variation. To avoid these problems, we compared the satellite-based metrics in 2020 with the multi-year average (2017–2019, without typhoons) to determine the disturbance of the typhoons on maize using LSWI with 8-day temporal resolution. The relative change ratio has been widely used to quantify vegetation disturbance (Hu & Smith, 2018; Peereman et al., 2020; M. Wang & Xu, 2018). To further achieve comparability among the LSWI, we calculated the relative interannual anomaly of LSWI as the typhoon disturbance on maize expressed as ΔLSWI (%). The ΔLSWI (%) for each pixel in 2020 was derived relative to the multiyear mean value from 2017 to 2019, as there were no extreme climate events in Northeast China during the three consecutive years. The ΔLSWI (%) of the regions of interest (ROIs) and the entire study region were calculated by averaging the pixels.

$$\Delta\mathrm{LSWI} = \frac{\mathrm{LSWI}_{2020} - \mathrm{LSWI}_{\mathrm{Baseline}}}{\mathrm{LSWI}_{\mathrm{Baseline}}} \times 100\% \tag{2}$$

$$\Delta\mathrm{LSWI}\,(\%) = \frac{\Delta\mathrm{LSWI}}{\mathrm{LSWI}_{\mathrm{max}} - \mathrm{LSWI}_{\mathrm{min}}} \tag{3}$$

where ΔLSWI (%) represents the relative interannual anomaly of LSWI to the typhoon disturbance on maize. LSWI_{2020} and $\mathrm{LSWI}_{\mathrm{Baseline}}$ refer to the LSWI value in 2020 and the mean LSWI value from 2017 to 2019, respectively. $\mathrm{LSWI}_{\mathrm{max}}$ and $\mathrm{LSWI}_{\mathrm{min}}$ are the maximum and minimum values of the LSWI seasonal variation in the baseline years, respectively. We used this normalization considering LSWI has a normal range between −1 and 1. The higher absolute values of ΔLSWI (%) mean higher sensitivity to typhoon disturbances. For comparison, we process other vegetation indices in a similar way.

2.6. Analysis of the Spatial Extent of Typhoon Disturbance on Maize

The intensity of typhoon disturbance varies greatly at the regional scale. Previous studies have found that the intensity of the typhoon disturbance decreases as it moves inland after landing (Chambers et al., 2007; Juárez et al., 2008). As the typhoon track distance increases, the intensity of the typhoon disturbance also gradually decreases (Ayala-Silva & Twumasi, 2004; X. Zhang et al., 2013). Therefore, we created buffers along the typhoon track from the coastline, and away from the track to analyze the spatial variations of typhoon disturbance on maize. The width of each buffer zone is 10 and 100 km, respectively, considering the interference of spatial heterogeneity. Here, we selected Typhoon Maysak as the research object because it is the most destructive with the longest impact duration (27 hr), almost crossing the entire maize region in Northeast China (Figure S5 and Table S1 in Supporting Information S1).

2.7. Machine Learning Models to Explore the Controlling Factors of the Impacts of Typhoons on Maize

We employed a RF algorithm to investigate the factors of the impacts of typhoon disturbance on maize. The variables included typhoon-related variables: distance away from the typhoon track, distance along the typhoon track, anomaly in total precipitation, and anomaly in maximum wind speed. We also included maize-related factors: the proportion of maize (data calculated based on You et al. (2021)) and the end of season (EOS, data available from Niu et al. (2022)). Environment-related factors were soil type, elevation, slope, and distance to the nearest forest. The data on typhoon-related variables were available from the CMSDC (http://data.cma.cn/) and the Typhoon Network of the Central Meteorological Observatory (http://typhoon.nmc.cn/). The distance along and away from the typhoon track here refers only to the distance from typhoon Maysak, due to it being the most destructive, having the longest path, and the longest residence time of the three typhoons. The soil type and elevation data were obtained from the Resource and Environment Science and Dara Center (https://www.resdc.cn/Default.aspx). The slope was calculated

based on the elevation. The forest map used to calculate the distance to the nearest forest was derived from Shimada et al.'s forest map (Shimada et al., 2014) with a 25-m resolution, which can better capture the small area of the forest.

Random forest regression is a supervised learning algorithm that uses an ensemble learning method for regression. It consists of multiple regression trees using bootstrapped samples. Each RF model consists of 100 regression trees with a leaf node size no smaller than 5 in our study. Split variables are randomly selected from all independent variables at each node of each tree, and the optimal branches are selected according to the branching superiority criterion. Then each regression tree starts top-down recursive branching until the splitting termination condition is satisfied. According to each variable's ability to increase the pureness of the leaves, each tree of the RF can be used to calculate the variable's importance. Averaging the variable importance factors of all the trees and normalizing them to unity for the RF model. We employed the ΔLSWI (%) as the proxy of maize lodging, that is, the dependent variable, and used typhoon, maize, and environment-related factors as the independent variables to train the RF model. We created random sample points using the maize layer (the maize proportion of maize is 0%–100%) and controlled the distance between each point to be greater than 5 km to avoid the influence of spatial autocorrelation (Karasiak et al., 2022), and finally we got 5,752 sample points (Figure S6 in Supporting Information S1). We randomly selected 70% of them as the training set and 30% as the testing set. To further strengthen the robustness of the results, we took the average of 100 RF results as the final importance level.

The response function of maize lodging to each factor is shown as a partial dependence plot (PDP). PDP is a graphical way to analyze and quantify the marginal effect of one independent variable (e.g., distance away from the typhoon track) on the target response (ΔLSWI (%)), allowing other variables to change in their domain. In practice, it can be approximated as:

$$\hat{f}_{x_s}(x_s) = \frac{1}{n}\sum_{i=1}^{n}\hat{f}\left(x_s, x_c^{(i)}\right) \tag{4}$$

where $\hat{f}_{x_s}$ is the partial dependent function of the variable x_s, $x_c^{(i)}$ is the value of the ith sample for the variable x_c.

3. Results

3.1. GEDI Footprints Reveal Changes in Maize Height Caused by Typhoons

We first generated maps of the physical height of maize before and after typhoons using GEDI waveform data (Figure 1). Figures 1a and 1b show that GEDI-based maize height was significantly reduced in part of the study area after three typhoon events. GEDI-based maize height was generally greater than 2.5 m before the typhoons (Figure 1a), but was lower than 2.3 m for regions close to the typhoon track after three typhoon events (Figure 1b). The central part of the study area, which was most severely affected by the typhoons, had a height of less than 2.1 m (Figure 1b). These numbers were much greater than zero even for the lodged maize due to the large GEDI laser pulse width, and 95th percentile of height signal being used (Methods). We also selected four regions of interest (ROIs, ~20 km × 20 km) to explore the spatial details in GEDI-based maize height changes before and after the typhoon events (Figures 1c and 1d). The four ROIs were selected considering that GEDI observations were obtained both before and after the typhoon events within these small areas, and they had a varying distance to the track of the most destructive typhoon, Maysak (Methods). We found that most of the GEDI-based canopy height in ROIs 1 and 2, which were closer to Maysak's track, dropped significantly after the typhoons. The post-typhoon canopy height was close to what it was after maize was harvested (Figures 1e and 1f). Considering no harvest activity was conducted within such a short time, and the canopy greenness remained nearly the same (Figures S4 and S7 in Supporting Information S1), such changes were most likely caused by the typhoon-induced crop lodging. ROIs 3 and 4 did not show a remarkable drop in GEDI-based heights after the typhoons, which suggested that there was little to no impact on maize in regions a long distance from the typhoon track (Figures 1g and 1h).

3.2. Wall-To-Wall Picture of Typhoon Disturbance on Maize Captured by Optical Metrics

Although GEDI LiDAR can characterize maize lodging immediately after typhoon disturbances, it does not provide highly resolved spatial details due to its coarse resolution (Dubayah et al., 2020). Thus, we incorporated LSWI from MODIS (W. Wang et al., 2010), a proxy of vegetation canopy water content, to depict the wall-to-wall pattern of the impacts of typhoons on maize. This metric takes advantage of the large contrast in canopy water changes between lodged and healthy maize: lodged maize shows a rapid decrease in canopy water content due to reduced xylem water transport while the healthy maize benefits from additional precipitation and the canopy

10.1029/2023EF003590

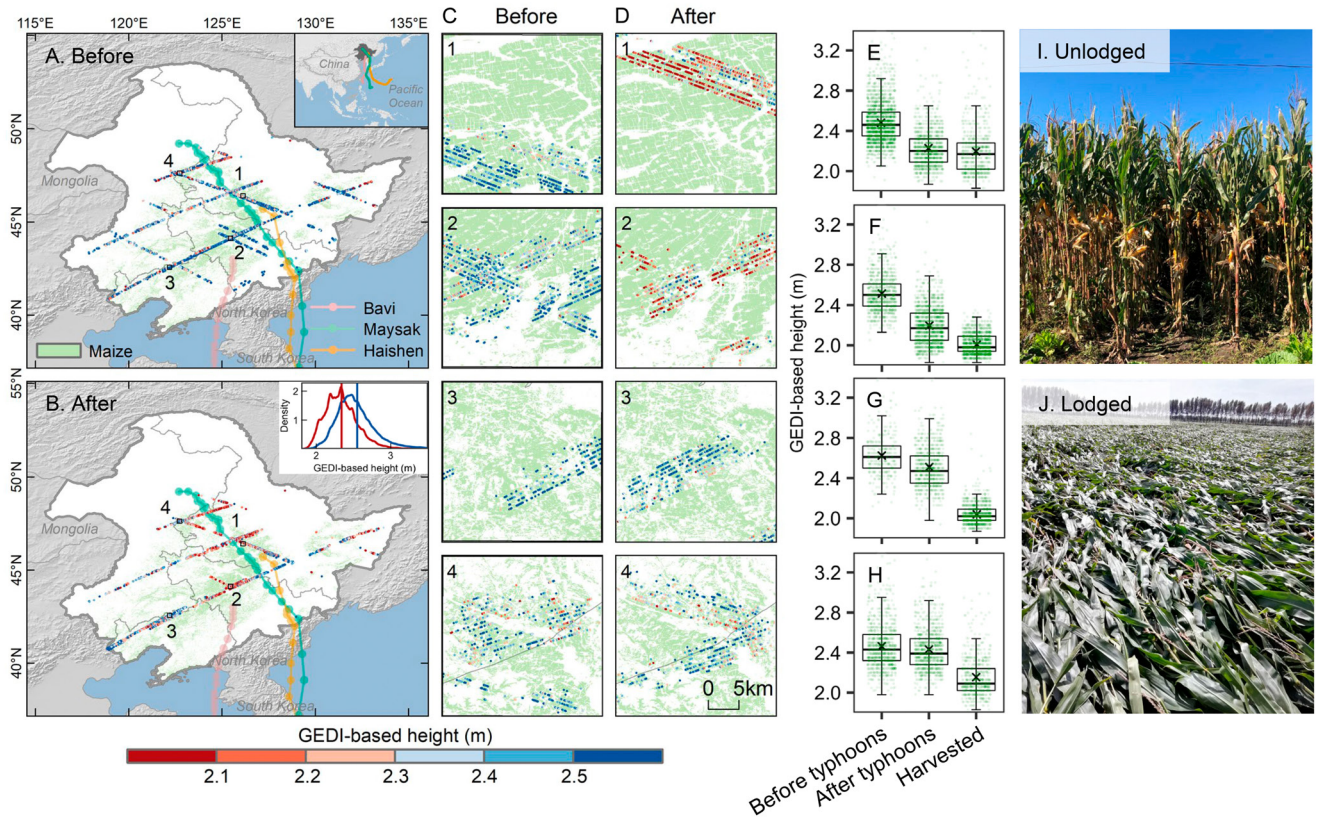

Figure 1. Depiction of maize height before and after the typhoons of 2020 in Northeast China by GEDI LiDAR. (a and b) Spatial patterns of GEDI-based maize height before (a) and after (b) the typhoons. The inset in panel (a) shows the location of the study area (gray polygon) and the three typhoon tracks in Monsoon Asia. The inset in panel (b) is the corresponding density diagrams of (a and b). The blue and red vertical lines indicate the mean values of GEDI-based maize height before and after the typhoons, respectively. (c and d) Detailed spatial patterns of GEDI-based maize height in the regions of interest (ROIs) before (c) and after (d) the typhoons, which are labeled in panels (a and b). ROI 1 is close to the Maysak track, ROI 2 is close to the Maysak track and coast, ROI 3 is close to the coast but far from the Maysak track, and ROI 4 is close to the Maysak track but deep inland. (e–h) GEDI-based maize height before and after the typhoons and after the maize harvested, corresponding to the ROI 1–4, respectively. It is worth noting that the number of GEDI footprints is different in each period due to a lack of revisits. Before typhoons means August 11–26, after typhoons means September 9–20, and harvested means December 1–15 in winter. (i and j) The in situ photographs of the landscape of unlodged (i) and lodged (j) maize.

water will increase (Chaves et al., 2002; Scoffoni et al., 2017). To better quantify the typhoon disturbance on maize, we calculated the relative interannual anomaly of LSWI (ΔLSWI (%)) as the change of maize growth caused by typhoons (Methods). We found that ΔLSWI (%) had a spatial pattern similar to GEDI-based maize height both before and after the typhoons (Figures 1 and 2). Heilongjiang and Jilin Provinces were the most affected by the typhoons, where ΔLSWI (%) decreased by more than 50% in some areas (Figures 2a and 2b). Conversely, the ΔLSWI (%) in most of Liaoning and eastern Inner Mongolia was positive where the typhoon impacts were limited (Figures 2a and 2b). For the ROIs mentioned in Figure 1, the mean ΔLSWI (%) of ROI 1 and ROI 2 were 0.14% and −2.14% before the typhoons (Figures 2c, 2e, and 2f), which dropped to −21.84% and −13.7% after the typhoons, respectively (Figures 2d–2f). In contrast, the mean ΔLSWI (%) of ROI 3 and ROI 4 before the typhoons were −0.49% and −2.06% (Figures 2c, 2g, and 2h), and increased to 13.59% and 13.04% after the typhoons, respectively (Figures 2d, 2g, and 2h). LSWI had an advantage over other optical indicators related to maize leaf area (NDVI and NIR_V), greenness (EVI), and canopy function (CSIF) (Figures S7–S11 in Supporting Information S1). The excellent consistency between GEDI data and optical metrics (e.g., LSWI) suggests that the optical metrics can reliably portray typhoon disturbances (Figures S12–S16 in Supporting Information S1).

3.3. Controlling Factors and Underlying Mechanisms

We further analyzed the spatial patterns of typhoon impacts on maize using ΔLSWI (%) (Figure 3). To do so, we first created multiple buffers of the coastline with 10 km intervals along the Maysak track, which was the

10.1029/2023EF003590

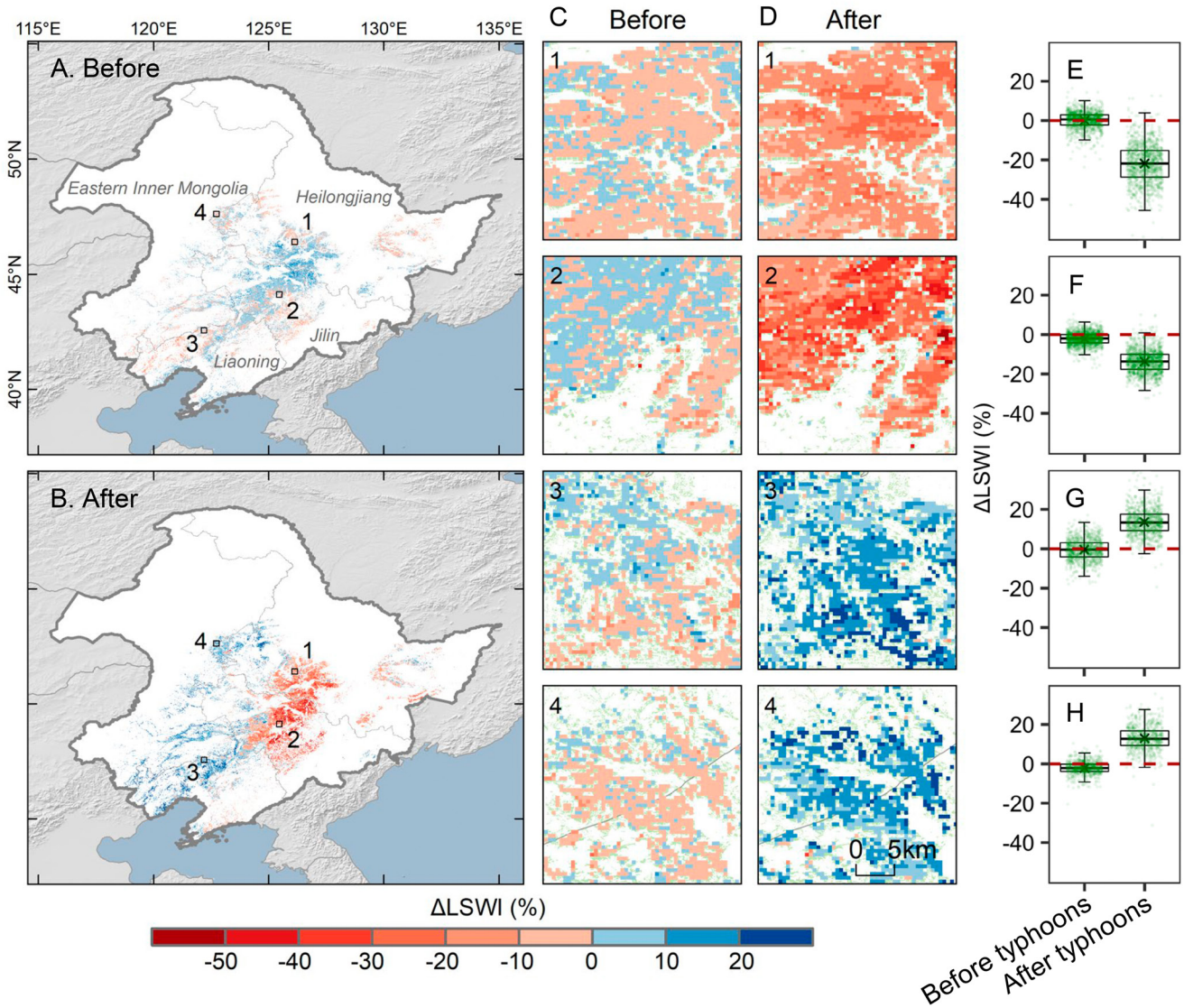

Figure 2. Wall-to-wall picture of typhoon disturbance on maize of 2020 in Northeast China. (a and b) Spatial patterns of normalized relative change ratio of land surface water index (ΔLSWI (%)) relative to the baseline years (2017–2019) before (a) and after (b) the typhoons. Spatial patterns of ΔEVI (%), ΔNIR_V (%), and ΔCSIF (%) are described in Figure S8–S11 of Supporting Information S1. (c and d) Detailed spatial patterns of ΔLSWI (%) in regions of interest (ROIs) before (c) and after (c) the typhoons, respectively, corresponding to the ROI 1–4 in Figures 1a and 1b. (e–h) The boxplots show the ΔLSWI (%) before and after the typhoons, corresponding to the ROI 1–4, respectively. The horizontal dotted line in panels (e–h) indicates ΔLSWI (%) equals zero.

longest-lasting and most destructive typhoon (Figure 3a). We found that the lodging increased and reached a maximum at around 400 km after landfall, and then decreased until ~550 km (Figure 3b). The area with the largest impact was in the range of ~300–~450 km along the track from the coast, which could be due to the greater wind speed, longer impact duration, and the flat terrain (Figures S3 and S17 in Supporting Information S1). This along-track disturbance pattern was also supported by one GEDI track, with a maximum impact at around 600 km. Such a mismatch between LSWI and GEDI may be explained by the fact that the GEDI track did not fully align with Maysak's track, and they intersected at around 600 km from the coast (Figure 3c). To evaluate the impact away from the typhoon, we generated multiple buffers parallel to Maysak's track (Figure 3a). We found the typhoon impacts were the largest within ~100 km of the track, and declined toward both directions when moving away from Maysak's track (Figure 3d). Similar patterns could also be observed using GEDI-based maize height (Figure 3e), as well as other optical metrics (Figures S18–S21 in Supporting Information S1). These analyses suggest that although the distance from the typhoon track is the primary factor determining typhoon-induced crop lodging, other factors may play important roles.

10.1029/2023EF003590

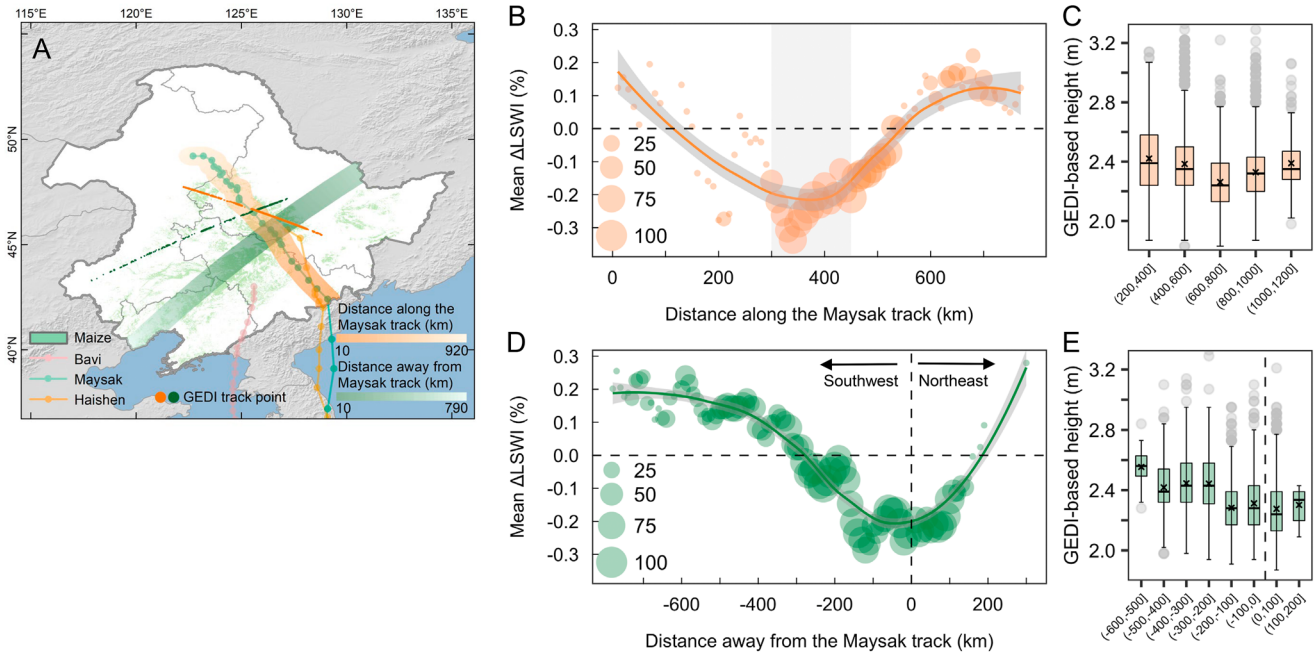

Figure 3. Spatial change of the typhoon disturbance on maize in 2020 in the study area. (a) Spatial distributions of the multiple buffers and GEDI track along and away from the Maysak track. Each buffer is 100 km long and 10 km wide. (b and c) Changes in ΔLSWI (%) (b) and GEDI-based height (c) with increasing distance along the Maysak track after the typhoons. (d and e) Changes in ΔLSWI (%) (d) and GEDI-based height (e) with increasing distance away from the Maysak track after the typhoons. Changes in ΔNDVI (%), ΔEVI (%), ΔNIR_V (%), and ΔCSIF (%) are described in Figures S18–S21 of Supporting Information S1. The size of the dots in panels (b and d) indicates the proportion of maize area (%) in each buffer zone.

To understand which factors contribute to crop lodging, we built a RF model and predicted the spatial patterns of ΔLSWI (%) using various variables related to characteristics of the typhoon, maize fraction, and local environment. LSWI provides enough samples to help us understand this question at the regional scale. The resulting model can explain 60.28% of the spatial out-of-bag variance for the impacts of typhoons on maize. Based on this model, we obtained the rank importance of variables that drive the spatial pattern, as well as their partial dependence (Figure 4).

As expected, typhoon-related factors played a dominant role in explaining the spatial patterns of lodging, with the two distance metrics explaining almost half of the variations (25.29%, away from the typhoon track; 22.87%, along the typhoon track) (Figure 4a). Lodging decreased further away from and along the typhoon track (Figures 3, 4b, and 4c). Precipitation and winds together explained ~16% of the variation (Figures 4a, 4e, and 4h). The contribution of these two factors increased to ~41% if we did not consider the two typhoon distance metrics (Figure S22 in Supporting Information S1). Maize-related factors, including the fraction of cropland occupied by maize and maize harvest date, explained 11.94% and 7.94% of the variation, respectively (Figure 4a). More severe lodging was found in areas with higher maize fractions (Figure 4d). Compared to other crop types, such as soybean, rice, and wheat, maize is much taller at this late growth stage and is more vulnerable to typhoons. Surprisingly, the maize with a later EOS, that is, those at the milk stage rather than maturity stage, exhibited greater loss, possibly due to higher water content and higher center of gravity so that they were less resistant to the strong wind (Figure 4f and Figure S4 in Supporting Information S1).

Environment-related factors, including elevation, soil type, slope of the terrain, and its distance from the nearest forest, also partly explained the typhoon-induced lodging (Figure 4a). Unlike studies that focus on the impact of typhoons on forests (Boose et al., 1994; Feng et al., 2020; Negrón-Juárez et al., 2014), terrain effects were often not the most important factor affecting crop lodging (Figure 4a), potentially because crops were mainly distributed in several major plains in our study area (Figures S2, S3, and S23 in Supporting Information S1). The role of soil type appeared relatively minor, with severe maize lodging primarily concentrated in areas featuring black and cinnamon soils, predominantly situated in the central part of Northeast China (Figures 4a and 4k, Figure S24 in Supporting Information S1). In these areas, typhoon-induced rainfall and wind were the dominant drivers

10.1029/2023EF003590

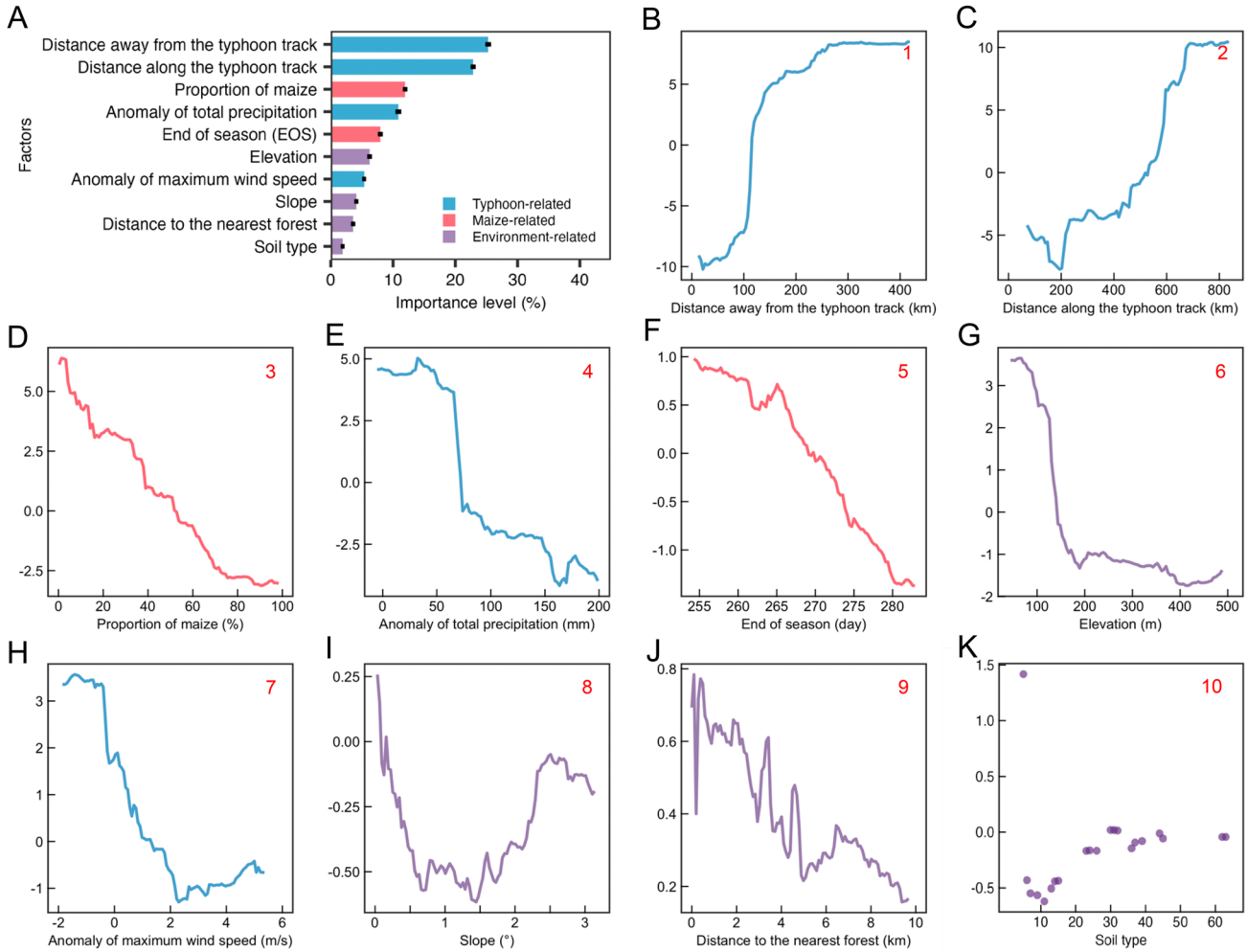

Figure 4. Response functions for the factors related to typhoon disturbance on maize. (a) Variable importance for predicting the degree of typhoon disturbance on maize. (b–k) Response functions obtained from the random forest models. The numbers in the top-right corners indicate the order of importance for predicting the degree of typhoon disturbance on maize. Note that the *x*-axis in panel (k) indicates the id of the soil type, which corresponds to the soil type in Table S2 of Supporting Information S1.

affecting maize. Although forests may weaken the wind speed within a certain range (Cai et al., 2021), this effect was small based on our analysis (Figure 4j). However, such an effect may be underestimated considering that the scattered shelterbelt forests may not be correctly identified in our forest map (Figures 4a and 4j). Further analysis using high-resolution forest maps and lodging maps may provide a more robust estimate.

3.4. Potential Increase of Lodging Risk With Maize Expansion

Climate change is expected to cause a poleward shift in typhoon occurrence (Altman et al., 2018; Elsner et al., 2008; Kossin, 2018; Tamarin-Brodsky & Kaspi, 2017), suggesting a potential increase in typhoon events in Northeast China. Surprisingly, we found a significant decline in typhoon density before 2010, this trend reversed and exhibited a strong increase during 2010–2020 (Figure 5a). As a direct indicator of typhoon intensity, the maximum wind speed showed a non-significant increase during the past 40 years (Figure 5b). Meanwhile, we found a steady increase in maize area since 1980, almost tripled over 40 years (Figure 5c). Considering maize is much more vulnerable than other vegetation types, this large expansion in the maize area can substantially elevate the lodging risk. Such increases may be further exacerbated by the contemporary delay of the maize maturity date, which extends the vulnerability period of maize when typhoon occurrence does not show a significant change (Figures 5d and 5e).

10.1029/2023EF003590

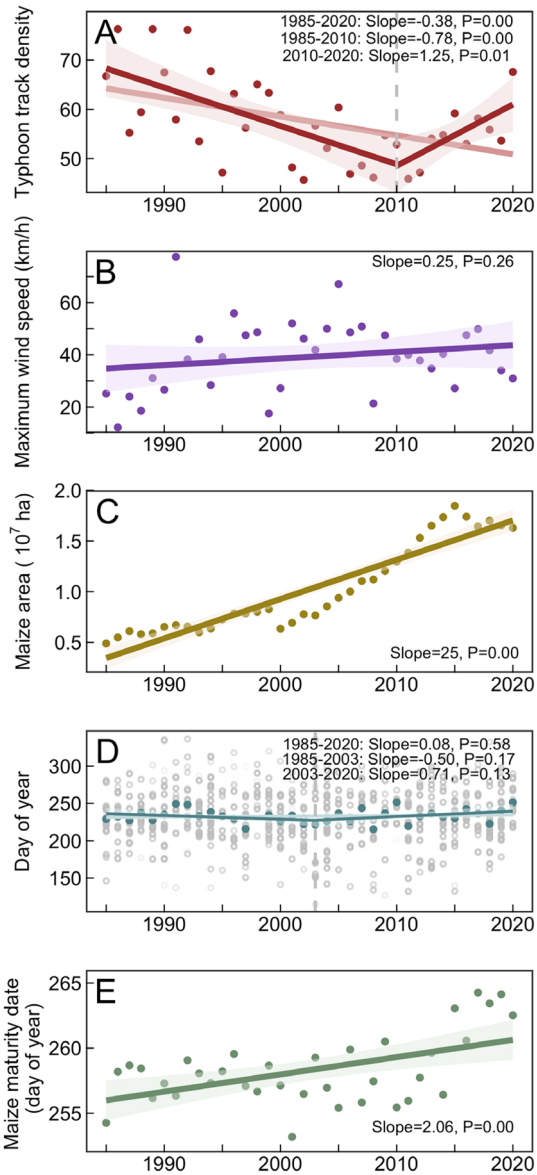

Figure 5. Temporal changes of typhoon and maize characteristics from 1985 to 2020 in Northeast Asia. The solid line is the best-fit line, and the shaded area is the 95% bootstrap confidence interval. The data on typhoon track density, average day of year for each year of typhoon occurrence, and maximum wind speed are taken from the International Best Track Archive for Climate Stewardship (IBTrACS) v03r05 (Knapp et al., 2010). The gray circles in panel (d) represent the day of year of each typhoon track. The data on maize area can be accessed from the National Bureau of Statistics, and maize maturity date data available from Niu et al. (2022).

4. Discussion

Crop lodging, usually caused by strong winds or heavy rainfall, has become an increasingly common agricultural hazard under global warming and more frequent extreme weather events (Baker et al., 2014; Berry et al., 2004). Lodging usually causes significant crop yield loss and considerable economic losses, which can be exacerbated by a series of domino effects, including physiological disorders, increased drying costs, reduced grain quality, and slowed harvest (Berry & Spink, 2012; Berry et al., 2013; Norberg et al., 1988; Setter et al., 1997). Traditional approaches to assessing crop lodging often face limitations such as restricted coverage, labor-intensive processes, restricted accessibility, and vulnerability to adverse weather conditions. Remote sensing technology can serve as a valuable complement to these traditional methods, offering the potential to enhance our understanding of crop lodging over broader spatial and temporal dimensions (Branson, 2011). The precise and timely detection of crop lodging, utilizing freely accessible remote sensing data with superior temporal and spatial resolutions, enables rapid monitoring of post-typhoon crop-affected regions on a large scale. This capability can significantly contribute to agricultural planning, facilitate agricultural insurance assessments, and inform policymaking processes.

Here, we used a combination of state-of-the-art satellite LiDAR and optical data to assess typhoon-induced maize lodging. Compared to other active or passive remote sensing techniques, LiDAR provided a direct measure of the canopy height and its changes can be regarded as the ground truth for crop lodging (Figure 1). Although GEDI was designed originally for forest ecosystems with a relatively large pulse width (14 ns) (Dubayah et al., 2020; Lang et al., 2022; Potapov et al., 2021), our study demonstrated that it can reliably track typhoon disturbance in our study area where the terrain is mostly flat. While it is undeniable that the GEDI footprint exhibits certain constraints in terms of both its temporal and spatial resolution, we believe that it adequately fulfills our assessment requirements. On one hand, following rigorous quality control measures for GEDI data, we successfully acquired more than 55,000 GEDI shots before and after the 2020 typhoons. These effectively encompass nearly the entirety of maize fields in Northeast China, providing a comprehensive depiction of the variations in maize canopy height following the typhoon's impact in this region. On the other hand, it is worth noting that despite GEDI's remarkable spatial resolution, approximately 25 m in diameter, it remains comparatively coarse when scrutinizing intricate crop structures. Consequently, we opted to aggregate the maize layer to a 50-m spatial resolution while excluding pixels with less than 50% maize content to align with the GEDI footprint. This strategic adjustment significantly mitigated the challenges posed by mixed pixels resulting from GEDI's relatively lower spatial resolution.

The limited spatial coverage of GEDI can be complemented by LSWI since it is sensitive to canopy water loss due to lodging-induced hydraulic failure (Gu et al., 2008; Jackson et al., 2004; Maki et al., 2004; Wagle et al., 2014; Xiao et al., 2004). Maize lodging indicated by a sharp decrease in LSWI may primarily pertain to the complete rupture of a stem or root, directly resulting in an obstruction of water uptake, consequently manifesting as a rapid decline in water content. Furthermore, it is worth noting that some maize plants may not lodge immediately upon the onset of a typhoon; instead, they may initially exhibit slight bending before eventually succumbing to lodging, which would manifest as a delayed decline in water content. This delayed lodging can be attributed to the fact that, following a typhoon, maize remains only slightly bent and capable of normal water absorption. However, the heavy rainfall accompanying the typhoon can weaken soil strength, potentially leading to root failure (Fan

et al., 2021). This, when coupled with strong winds, increases the self-weight moment acting on the crop at the stem base, thereby precipitating the fracture of the maize stalk or root (Sylvester-Bradley et al., 1990). During this process, there may be a transient increase in water content due to heightened water uptake by the corn plant. The maize disturbance pattern described by LSWI is similar to that of GEDI, both for the four ROIs and at the regional scale (Figures 1–3). The correlation analysis also showed their consistency at the GEDI track scale (Figures S12–S16 in Supporting Information S1). The combined use of LiDAR and LSWI can well portray a reliable and more comprehensive picture of maize lodging. The spatial distribution of maize yield variations also exhibited a consistent pattern with the GEDI- and LSWI-based maize lodging (Figures 1 and 2 and Figure S25 in Supporting Information S1). The areas experiencing significant declines in maize yield predominantly clustered in the central region of Northeast China in 2020. This central area encompasses cities in southwestern Heilongjiang Province and northern Jilin Province and is largely consistent with the areas shown by GEDI and LSWI to be severely affected by the typhoon.

Although the risk of maize lodging is expected to increase as maize croplands expand, multiple approaches may be made to reduce such a risk. Shelterbelt forests have been demonstrated to successfully reduce the impact of typhoons on crops at the local scale (Cai et al., 2021). For example, it can reduce typhoon-induced rice lodging to 16.28%, one-third of that without a shelterbelt (J. Zhang et al., 1996). Our analyses based on RF also demonstrated that forests have a mitigating effect on typhoon impacts at the regional scale (Figures 4a and 4j). However, this effect diminishes as we move away from the forest. An optimal shelterbelt forest density should consider a balance between the protection efficiency and the forest area.

In addition to the factors involved in our study (typhoon, maize, and environment-related factors), maize cultivars and crop management factors may also play an essential role in alleviating typhoon-induced maize lodging (Chauhan et al., 2019). The lodging-resistant varieties will have a higher stem diameter coefficient, internode puncture strength, and crushing strength of the basal internode, which can better resist strong winds (Tong et al., 2020). Moreover, crop management plans, such as sowing date, planting density, and tillage practices, may also reduce crop lodging. For example, altering the sowing dates can shift the maize to a more wind-resistant phenological stage when typhoons are most active (Ciampitti et al., 2011; Kirby et al., 1985; Milford et al., 1993; Spink et al., 2000). Also, reducing stem density can alleviate competition for limited resources such as light, decrease plant height, and reduce the risk of lodging (Sangoi et al., 2002; Van Roekel & Coulter, 2011). Rotary tillage before seeding could also effectively increase the lodging resistance by lowering the center of gravity and increasing the root anchoring strength (Bian et al., 2016).

Typhoons are projected to migrate poleward and intensify under global warming (Altman et al., 2018; Elsner et al., 2008; Kossin, 2018; Kossin et al., 2014; Tamarin-Brodsky & Kaspi, 2017) (Figure 5). The spatial co-occurrence of these climate extremes may simultaneously threaten the global mid-and high-latitude major breadbasket regions at the same time, further threatening global food security, which can lead to conflict, war, and demographic pressure (Godfray et al., 2010; Jägermeyr et al., 2020; X.-Y. Li et al., 2022). Improvements in crop lodging monitoring systems and mitigation practices are critical for reducing the impact of climate change on global maize yields.

Data Availability Statement

The GEDI L2A data set is available from Dubayah et al. (2021). The MCD43A4 collection 6 data set is available from Schaaf and Wang (2015). The CSIF data set used in the analysis can be accessed from Y. Zhang (2018). The annual maps of maize are available from You et al. (2021). Tropical cyclone data were taken from the International Best Track Archive for Climate Stewardship (Knapp et al., 2010, 2018). All the scripts for the data analyses are available on Zenodo (Q. Zhang et al., 2023).

Acknowledgments
This research is supported by the National Natural Science Foundation of China (Nos. 42171115, 42271375, and 72221002), the Strategic Priority Research Program of the Chinese Academy of Sciences (XDA28060100), the Youth Interdisciplinary Team Project of the Chinese Academy of Sciences (JCTD-2021-04), and the 2115 Talent Development Program of China Agricultural University.

References

Abbas, S., Nichol, J. E., Fischer, G. A., Wong, M. S., & Irteza, S. M. (2020). Impact assessment of a super-typhoon on Hong Kong's secondary vegetation and recommendations for restoration of resilience in the forest succession. *Agricultural and Forest Meteorology*, *280*, 107784. https://doi.org/10.1016/j.agrformet.2019.107784

Altman, J., Ukhvatkina Olga, N., Omelko Alexander, M., Macek, M., Plener, T., Pejcha, V., et al. (2018). Poleward migration of the destructive effects of tropical cyclones during the 20th century. *Proceedings of the National Academy of Sciences*, *115*(45), 11543–11548. https://doi.org/10.1073/pnas.1808979115

Ayala-Silva, T., & Twumasi, Y. A. (2004). Hurricane Georges and vegetation change in Puerto Rico using AVHRR satellite data. *International Journal of Remote Sensing*, *25*(9), 1629–1640. https://doi.org/10.1080/01431160310001595037

Baker, C. J., Sterling, M., & Berry, P. (2014). A generalised model of crop lodging. *Journal of Theoretical Biology*, *363*, 1–12. https://doi.org/10.1016/j.jtbi.2014.07.032

Berry, P., White, C., Sterling, M., & Baker, C. (2013). Development of a model of lodging risk in oilseed rape to enable integrated lodging control to reduce PGR use. *CRD Project PS2146*.

Berry, P. M., & Spink, J. (2012). Predicting yield losses caused by lodging in wheat. *Field Crops Research*, *137*, 19–26. https://doi.org/10.1016/j.fcr.2012.07.019

Berry, P. M., Sterling, M., Spink, J. H., Baker, C. J., Sylvester-Bradley, R., Mooney, S. J., et al. (2004). Understanding and reducing lodging in cereals. In *Advances in agronomy* (Vol. 84, pp. 217–271). Academic Press.

Bian, D. H., Jia, G. P., Cai, L. J., Ma, Z. Y., Eneji, A. E., & Cui, Y. H. (2016). Effects of tillage practices on root characteristics and root lodging resistance of maize. *Field Crops Research*, *185*, 89–96. https://doi.org/10.1016/j.fcr.2015.10.008

Boose, E. R., Foster, D. R., & Fluet, M. (1994). Hurricane impacts to tropical and temperate forest landscapes. *Ecological Monographs*, *64*(4), 369–400. https://doi.org/10.2307/2937142

Boutet, J. C., & Weishampel, J. F. (2003). Spatial pattern analysis of pre- and post-hurricane forest canopy structure in North Carolina, USA. *Landscape Ecology*, *18*(6), 553–559. https://doi.org/10.1023/A:1026058312853

Brandt, M., Hiernaux, P., Rasmussen, K., Mbow, C., Kergoat, L., Tagesson, T., et al. (2016). Assessing woody vegetation trends in Sahelian drylands using MODIS based seasonal metrics. *Remote Sensing of Environment*, *183*, 215–225. https://doi.org/10.1016/j.rse.2016.05.027

Branson, M. (2011). Using conservation agriculture and precision agriculture to improve a farming system. *Rainfed Farming Systems*, 875–900. https://doi.org/10.1007/978-1-4020-9132-2_34

Cai, X., Henderson, M., Wang, L., Su, Y., & Liu, B. (2021). Shelterbelt structure and crop protection from increased typhoon activity in Northeast China. *Agriculture*, *11*(10), 995. https://doi.org/10.3390/agriculture11100995

Chambers, J. Q., Fisher, J. I., Zeng, H., Chapman, E. L., Baker, D. B., & Hurtt, G. C. (2007). Hurricane Katrina's carbon footprint on U.S. Gulf Coast forests. *Science*, *318*(5853), 1107. https://doi.org/10.1126/science.1148913

Chauhan, S., Darvishzadeh, R., Boschetti, M., Pepe, M., & Nelson, A. (2019). Remote sensing-based crop lodging assessment: Current status and perspectives. *ISPRS Journal of Photogrammetry and Remote Sensing*, *151*, 124–140. https://doi.org/10.1016/j.isprsjprs.2019.03.005

Chaves, M. M., Pereira, J. S., Maroco, J., Rodrigues, M. L., Ricardo, C. P. P., Osorio, M. L., et al. (2002). How plants cope with water stress in the field. Photosynthesis and growth. *Annals of Botany*, *89*(7), 907–916. https://doi.org/10.1093/aob/mcf105

Ciampitti, I. A., Elmore, R. W., & Lauer, J. (2011). Corn growth and development. *Dent*, *5*, 75.

de Beurs, K. M., McThompson, N. S., Owsley, B. C., & Henebry, G. M. (2019). Hurricane damage detection on four major Caribbean islands. *Remote Sensing of Environment*, *229*, 1–13. https://doi.org/10.1016/j.rse.2019.04.028

Dubayah, R., Blair, J. B., Goetz, S., Fatoyinbo, L., Hansen, M., Healey, S., et al. (2020). The Global Ecosystem Dynamics Investigation: High-resolution laser ranging of the Earth's forests and topography. *Science of Remote Sensing*, *1*, 100002. https://doi.org/10.1016/j.srs.2020.100002

Dubayah, R., Hofton, M., Blair, J., Armston, J., Tang, H., & Luthcke, S. (2021). GEDI L2A Elevation and Height Metrics Data Global Footprint Level V002 [Dataset]. NASA EOSDIS Land Processes Distributed Active Archive Center. https://doi.org/10.5067/GEDI/GEDI02_A.002

Elsner, J. B., Kossin, J. P., & Jagger, T. H. (2008). The increasing intensity of the strongest tropical cyclones. *Nature*, *455*(7209), 92–95. https://doi.org/10.1038/nature07234

Emanuel, K. (2005). Increasing destructiveness of tropical cyclones over the past 30 years. *Nature*, *436*(7051), 686–688. https://doi.org/10.1038/nature03906

Fan, C.-C., Lu, J. Z., & Chen, H. H. (2021). The pullout resistance of plant roots in the field at different soil water conditions and root geometries. *Catena*, *207*, 105593. https://doi.org/10.1016/j.catena.2021.105593

Feng, Y., Negrón-Juárez, R. I., & Chambers, J. Q. (2020). Remote sensing and statistical analysis of the effects of Hurricane María on the forests of Puerto Rico. *Remote Sensing of Environment*, *247*, 111940. https://doi.org/10.1016/j.rse.2020.111940

Ghil, M., & Vautard, R. (1991). Interdecadal oscillations and the warming trend in global temperature time series. *Nature*, *350*(6316), 324–327. https://doi.org/10.1038/350324a0

Godfray, H. C. J., Beddington John, R., Crute Ian, R., Haddad, L., Lawrence, D., Muir James, F., et al. (2010). Food security: The challenge of feeding 9 billion people. *Science*, *327*(5967), 812–818. https://doi.org/10.1126/science.1185383

Gu, Y., Hunt, E., Wardlow, B., Basara, J. B., Brown, J. F., & Verdin, J. P. (2008). Evaluation of MODIS NDVI and NDWI for vegetation drought monitoring using Oklahoma Mesonet soil moisture data. *Geophysical Research Letters*, *35*(22), L22401. https://doi.org/10.1029/2008GL035772

Hasegawa, T., Sakurai, G., Fujimori, S., Takahashi, K., Hijioka, Y., & Masui, T. (2021). Extreme climate events increase risk of global food insecurity and adaptation needs. *Nature Food*, *2*(8), 587–595. https://doi.org/10.1038/s43016-021-00335-4

Hilker, T., Lyapustin, A. I., Tucker, C. J., Sellers, P. J., Hall, F. G., & Wang, Y. (2012). Remote sensing of tropical ecosystems: Atmospheric correction and cloud masking matter. *Remote Sensing of Environment*, *127*, 370–384. https://doi.org/10.1016/j.rse.2012.08.035

Hu, T., & Smith, R. B. (2018). The impact of Hurricane Maria on the vegetation of Dominica and Puerto Rico using multispectral remote sensing. *Remote Sensing*, *10*(6), 827. https://doi.org/10.3390/rs10060827

Jackson, T. J., Chen, D., Cosh, M., Li, F., Anderson, M., Walthall, C., et al. (2004). Vegetation water content mapping using Landsat data derived normalized difference water index for corn and soybeans. *Remote Sensing of Environment*, *92*(4), 475–482. https://doi.org/10.1016/j.rse.2003.10.021

Jägermeyr, J., Robock, A., Elliott, J., Müller, C., Xia, L., Khabarov, N., et al. (2020). A regional nuclear conflict would compromise global food security. *Proceedings of the National Academy of Sciences*, *117*(13), 7071–7081. https://doi.org/10.1073/pnas.1919049117

Juárez, R. I. N., Chambers, J. Q., Zeng, H., & Baker, D. B. (2008). Hurricane driven changes in land cover create biogeophysical climate feedbacks. *Geophysical Research Letters*, *35*(23), L23401. https://doi.org/10.1029/2008gl035683

Karasiak, N., Dejoux, J. F., Monteil, C., & Sheeren, D. (2022). Spatial dependence between training and test sets: Another pitfall of classification accuracy assessment in remote sensing. *Machine Learning*, *111*(7), 2715–2740. https://doi.org/10.1007/s10994-021-05972-1

Kirby, E. J. M., Appleyard, M., & Fellowes, G. (1985). Variation in development of wheat and barley in response to sowing date and variety. *The Journal of Agricultural Science*, *104*(2), 383–396. https://doi.org/10.1017/s0021859600044075

Knapp, K. R., Diamond, H. J., Kossin, J. P., Kruk, M. C., & Schreck, C. J. (2018). International Best Track Archive for Climate Stewardship (IBTrACS) Project, Version 4 [Dataset]. NOAA National Centers for Environmental Information. https://www.ncei.noaa.gov/data/international-best-track-archive-for-climate-stewardship-ibtracs/v04r00/access/shapefile/

Knapp, K. R., Kruk, M. C., Levinson, D. H., Diamond, H. J., & Neumann, C. J. (2010). The International Best Track Archive for Climate Stewardship (IBTrACS): Unifying tropical cyclone data. *Bulletin of the American Meteorological Society*, *91*(3), 363–376. https://doi.org/10.1175/2009bams2755.1

Kossin, J. P. (2018). A global slowdown of tropical-cyclone translation speed. *Nature*, *558*(7708), 104–107. https://doi.org/10.1038/s41586-018-0158-3

Kossin, J. P., Emanuel, K. A., & Vecchi, G. A. (2014). The poleward migration of the location of tropical cyclone maximum intensity. *Nature*, *509*(7500), 349–352. https://doi.org/10.1038/nature13278

Kupfer, J. A., Myers, A. T., McLane, S. E., & Melton, G. N. (2008). Patterns of forest damage in a southern Mississippi landscape caused by Hurricane Katrina. *Ecosystems*, *11*(1), 45–60. https://doi.org/10.1007/s10021-007-9106-z

Lang, N., Kalischek, N., Armston, J., Schindler, K., Dubayah, R., & Wegner, J. D. (2022). Global canopy height regression and uncertainty estimation from GEDI LIDAR waveforms with deep ensembles. *Remote Sensing of Environment*, *268*, 112760. https://doi.org/10.1016/j.rse.2021.112760

Lesk, C., Rowhani, P., & Ramankutty, N. (2016). Influence of extreme weather disasters on global crop production. *Nature*, *529*(7584), 84–87. https://doi.org/10.1038/nature16467

Li, K., & Li, G. (2011). Vulnerability assessment of storm surges in the coastal area of Guangdong Province. *Natural Hazards and Earth System Sciences*, *11*(7), 2003–2010. https://doi.org/10.5194/nhess-11-2003-2011

Li, X.-Y., Li, X., Fan, Z., Mi, L., Kandakji, T., Song, Z., et al. (2022). Civil war hinders crop production and threatens food security in Syria. *Nature Food*, *3*(1), 38–46. https://doi.org/10.1038/s43016-021-00432-4

Li, Z., Huang, C., Zhu, Z., Gao, F., Tang, H., Xin, X., et al. (2018). Mapping daily leaf area index at 30 m resolution over a meadow steppe area by fusing Landsat, Sentinel-2A and MODIS data. *International Journal of Remote Sensing*, *39*(23), 9025–9053. https://doi.org/10.1080/01431161.2018.1504342

Maki, M., Ishiahra, M., & Tamura, M. (2004). Estimation of leaf water status to monitor the risk of forest fires by using remotely sensed data. *Remote Sensing of Environment*, *90*(4), 441–450. https://doi.org/10.1016/j.rse.2004.02.002

McNulty, S. G. (2002). Hurricane impacts on US forest carbon sequestration. *Environmental Pollution*, *116*, S17–S24. https://doi.org/10.1016/s0269-7491(01)00242-1

Mei, W., & Xie, S.-P. (2016). Intensification of landfalling typhoons over the northwest Pacific since the late 1970s. *Nature Geoscience*, *9*(10), 753–757. https://doi.org/10.1038/ngeo2792

Mendelsohn, R., Emanuel, K., Chonabayashi, S., & Bakkensen, L. (2012). The impact of climate change on global tropical cyclone damage. *Nature Climate Change*, *2*(3), 205–209. https://doi.org/10.1038/nclimate1357

Milford, G. F. J., Penny, A., Prew, R. D., Darby, R. J., & Todd, A. D. (1993). Effects of previous crop, sowing date, and winter and spring applications of nitrogen on the growth, nitrogen uptake and yield of winter wheat. *The Journal of Agricultural Science*, *121*(1), 1–12. https://doi.org/10.1017/s0021859600076735

Negrón-Juárez, R., Baker, D. B., Chambers, J. Q., Hurtt, G. C., & Goosem, S. (2014). Multi-scale sensitivity of Landsat and MODIS to forest disturbance associated with tropical cyclones. *Remote Sensing of Environment*, *140*, 679–689. https://doi.org/10.1016/j.rse.2013.09.028

Niu, Q. D., Li, X. C., Huang, J. X., Huang, H., Huang, X. D., Su, W., & Yuan, W. P. (2022). A 30 m annual maize phenology dataset from 1985 to 2020 in China. *Earth System Science Data*, *14*(6), 2851–2864. https://doi.org/10.5194/essd-14-2851-2022

Norberg, O. S., Mason, S. C., & Lowry, S. R. (1988). Ethephon influence on harvestable yield, grain quality, and lodging of corn. *Agronomy Journal*, *80*(5), 768–772. https://doi.org/10.2134/agronj1988.00021962008000050015x

Norris, J. R., & Walker, J. J. (2020). Solar and sensor geometry, not vegetation response, drive satellite NDVI phenology in widespread ecosystems of the western United States. *Remote Sensing of Environment*, *249*, 112013. https://doi.org/10.1016/j.rse.2020.112013

Oliver, M. A., & Webster, R. (1990). Kriging: A method of interpolation for geographical information systems. *International Journal of Geographical Information Systems*, *4*(3), 313–332. https://doi.org/10.1080/02693799008941549

Parry, M. L., & Carter, T. R. (1989). An assessment of the effects of climatic change on agriculture. *Climatic Change*, *15*(1), 95–116. https://doi.org/10.1007/BF00138848

Peereman, J., Hogan, J. A., & Lin, T.-C. (2020). Assessing typhoon-induced canopy damage using vegetation indices in the Fushan Experimental Forest, Taiwan. *Remote Sensing*, *12*(10), 1654. https://doi.org/10.3390/rs12101654

Pinthus, M. J. (1974). Lodging in wheat, barley, and oats: The phenomenon, its causes, and preventive measures. *Advances in Agronomy*, *25*, 209–263. https://doi.org/10.1016/s0065-2113(08)60782-8

Potapov, P., Li, X., Hernandez-Serna, A., Tyukavina, A., Hansen, M. C., Kommareddy, A., et al. (2021). Mapping global forest canopy height through integration of GEDI and Landsat data. *Remote Sensing of Environment*, *253*, 112165. https://doi.org/10.1016/j.rse.2020.112165

Ray, D. K., Sloat, L. L., Garcia, A. S., Davis, K. F., Ali, T., & Xie, W. (2022). Crop harvests for direct food use insufficient to meet the UN's food security goal. *Nature Food*, *3*(5), 367–374. https://doi.org/10.1038/s43016-022-00504-z

Rogan, J., Schneider, L., Christman, Z., Millones, M., Lawrence, D., & Schmook, B. (2011). Hurricane disturbance mapping using MODIS EVI data in the southeastern Yucatán, Mexico. *Remote Sensing Letters*, *2*(3), 259–267. https://doi.org/10.1080/01431161.2010.520344

Roser, M., Ritchie, H., & Ortiz-Ospina, E. (2013). World population growth. *Our world in data*.

Sangoi, L., Gracietti, M. A., Rampazzo, C., & Bianchetti, P. (2002). Response of Brazilian maize hybrids from different eras to changes in plant density. *Field Crops Research*, *79*(1), 39–51. https://doi.org/10.1016/s0378-4290(02)00124-7

Schaaf, C., & Wang, Z. (2015). MCD43A4 MODIS/Terra+Aqua BRDF/Albedo Nadir BRDF Adjusted Ref Daily L3 Global - 500m V006 [Dataset]. NASA EOSDIS Land Processes Distributed Active Archive Center. https://doi.org/10.5067/MODIS/MCD43A4.006

Schaaf, C. B., Gao, F., Strahler, A. H., Lucht, W., Li, X., Tsang, T., et al. (2002). First operational BRDF, albedo nadir reflectance products from MODIS. *Remote Sensing of Environment*, *83*(1), 135–148. https://doi.org/10.1016/s0034-4257(02)00091-3

Scoffoni, C., Albuquerque, C., Brodersen, C. R., Townes, S. V., John, G. P., Bartlett, M. K., et al. (2017). Outside-xylem vulnerability, not xylem embolism, controls leaf hydraulic decline during dehydration. *Plant Physiology*, *173*(2), 1197–1210. https://doi.org/10.1104/pp.16.01643

Setter, T. L., Laureles, E. V., & Mazaredo, A. M. (1997). Lodging reduces yield of rice by self-shading and reductions in canopy photosynthesis. *Field Crops Research*, *49*(2), 95–106. https://doi.org/10.1016/s0378-4290(96)01058-1

Sharmila, S., & Walsh, K. J. E. (2018). Recent poleward shift of tropical cyclone formation linked to Hadley cell expansion. *Nature Climate Change*, *8*(8), 730–736. https://doi.org/10.1038/s41558-018-0227-5

Shekhar, A., Buchmann, N., & Gharun, M. (2022). How well do recently reconstructed solar-induced fluorescence datasets model gross primary productivity? *Remote Sensing of Environment*, *283*, 113282. https://doi.org/10.1016/j.rse.2022.113282

Shimada, M., Itoh, T., Motooka, T., Watanabe, M., Shiraishi, T., Thapa, R., & Lucas, R. (2014). New global forest/non-forest maps from ALOS PALSAR data (2007–2010). *Remote Sensing of Environment*, *155*, 13–31. https://doi.org/10.1016/j.rse.2014.04.014

Solomon, S., Plattner, G.-K., Knutti, R., & Friedlingstein, P. (2009). Irreversible climate change due to carbon dioxide emissions. *Proceedings of the National Academy of Sciences*, *106*(6), 1704–1709. https://doi.org/10.1073/pnas.0812721106

Spink, J., Whaley, J., Wade, A., Sparkes, D., & Foulkes, J. (2000). Prediction of optimum plant population in winter wheat (p. 234).

Studholme, J., Fedorov, A. V., Gulev, S. K., Emanuel, K., & Hodges, K. (2022). Poleward expansion of tropical cyclone latitudes in warming climates. *Nature Geoscience*, *15*(1), 14–28. https://doi.org/10.1038/s41561-021-00859-1

Sylvester-Bradley, R., Scott, R., & Wright, C. (1990). Physiology in the production and improvement of cereals (p. 18).

Tamarin-Brodsky, T., & Kaspi, Y. (2017). Enhanced poleward propagation of storms under climate change. *Nature Geoscience*, *10*(12), 908–913. https://doi.org/10.1038/s41561-017-0001-8

Tong, S., Du, Z., Li, C., & Song, F. (2020). Comparison of stem characteristics and screening of lodging resistance varieties in Sanjiang Plain. *Molecular Plant Breeding*, *18*(17), 5860–5868.

Tran, T. V., de Beurs, K. M., & Julian, J. P. (2016). Monitoring forest disturbances in Southeast Oklahoma using Landsat and MODIS images. *International journal of applied earth observation and geoinformation*, *44*, 42–52. https://doi.org/10.1016/j.jag.2015.07.001

van Dijk, M., Morley, T., Rau, M. L., & Saghai, Y. (2021). A meta-analysis of projected global food demand and population at risk of hunger for the period 2010–2050. *Nature Food*, *2*(7), 494–501. https://doi.org/10.1038/s43016-021-00322-9

Van Roekel, R. J., & Coulter, J. A. (2011). Agronomic responses of corn to planting date and plant density. *Agronomy Journal*, *103*(5), 1414–1422. https://doi.org/10.2134/agronj2011.0071

Wagle, P., Xiao, X., Torn, M. S., Cook, D. R., Matamala, R., Fischer, M. L., et al. (2014). Sensitivity of vegetation indices and gross primary production of tallgrass prairie to severe drought. *Remote Sensing of Environment*, *152*, 1–14. https://doi.org/10.1016/j.rse.2014.05.010

Wang, F., & Xu, Y. J. (2009). Hurricane Katrina-induced forest damage in relation to ecological factors at landscape scale. *Environmental Monitoring and Assessment*, *156*(1), 491–507. https://doi.org/10.1007/s10661-008-0500-6

Wang, M., & Xu, H. (2018). Remote sensing-based assessment of vegetation damage by a strong typhoon (Meranti) in Xiamen Island, China. *Natural Hazards*, *93*(3), 1231–1249. https://doi.org/10.1007/s11069-018-3351-7

Wang, W., Qu, J. J., Hao, X., Liu, Y., & Stanturf, J. A. (2010). Post-hurricane forest damage assessment using satellite remote sensing. *Agricultural and Forest Meteorology*, *150*(1), 122–132. https://doi.org/10.1016/j.agrformet.2009.09.009

Webster, P. J., Holland, G. J., Curry, J. A., & Chang, H. R. (2005). Changes in tropical cyclone number, duration, and intensity in a warming environment. *Science*, *309*(5742), 1844–1846. https://doi.org/10.1126/science.1116448

Weinkle, J., Landsea, C., Collins, D., Musulin, R., Crompton, R. P., Klotzbach, P. J., & Pielke, R. (2018). Normalized hurricane damage in the continental United States 1900–2017. *Nature Sustainability*, *1*(12), 808–813. https://doi.org/10.1038/s41893-018-0165-2

Xiao, X., Hollinger, D., Aber, J., Goltz, M., Davidson, E. A., Zhang, Q., & Moore, B. (2004). Satellite-based modeling of gross primary production in an evergreen needleleaf forest. *Remote Sensing of Environment*, *89*(4), 519–534. https://doi.org/10.1016/j.rse.2003.11.008

You, N., Dong, J., Huang, J., Du, G., Zhang, G., He, Y., et al. (2021). The 10-m crop type maps in Northeast China during 2017-2019. *Scientific Data*, *8*(1), 41. https://doi.org/10.1038/s41597-021-00827-9

Zhang, J., Kang, L., & Ji, Y. (1996). Effect of farmland windbreak on preventing rice lodging and yield reduction under violent tropical storm. *Chinese Journal of Applied Ecology*, *7*(1), 15.

Zhang, Q., Zhang, G., Zhang, Y., Xiao, X., You, N., Li, Z., et al. (2023). Increasing typhoon threats to the expanding maize fields in Northeast China [Software]. Zenodo. https://doi.org/10.5281/zenodo.7652183

Zhang, X., Wang, Y., Jiang, H., & Wang, X. (2013). Remote-sensing assessment of forest damage by Typhoon Saomai and its related factors at landscape scale. *International Journal of Remote Sensing*, *34*(21), 7874–7886. https://doi.org/10.1080/01431161.2013.827344

Zhang, Y. (2018). CSIF (Version 2) [Dataset]. Figshare. https://doi.org/10.6084/m9.figshare.6387494.v2

Zhang, Y., Joiner, J., Alemohammad, S. H., Zhou, S., & Gentine, P. (2018). A global spatially contiguous solar-induced fluorescence (CSIF) dataset using neural networks. *Biogeosciences*, *15*(19), 5779–5800. https://doi.org/10.5194/bg-15-5779-2018

Zhang, Y., Xiao, X., Zhang, Y., Wolf, S., Zhou, S., Joiner, J., et al. (2018). On the relationship between sub-daily instantaneous and daily total gross primary production: Implications for interpreting satellite-based SIF retrievals. *Remote Sensing of Environment*, *205*, 276–289. https://doi.org/10.1016/j.rse.2017.12.009